Nuclear Science and Techniques (2023) 34:29
https://doi.org/10.1007/s41365-023-01181-8

Assessment of the induced radioactivity in the treatment room of the heavy-ion medical machine in Wuwei using PHITS

Ying Luo[1,2,3,4] · Sheng-Cong Huang[1,2,3,4] · Hui Zhang[1,2,3,4] · Hai-Jun Mao[1,5] · Qiang Li[1,2,3,4] · Zhong-Ying Dai[1,2,3,4]

Received: 11 September 2022 / Revised: 15 December 2022 / Accepted: 16 December 2022 / Published online: 28 February 2023

Abstract

Carbon-ion radiotherapy (CIRT) offers unique physical and biological advantages over photon radiotherapy. However, some materials and devices in the CIRT treatment room become radioactive under bombardment by therapeutic carbon-ion beams due to nuclear reactions, thereby leading to possible radiation hazards to medical staff and additional and unwanted doses to patients. This study assessed the level of induced radioactivity in the treatment room of the Heavy-Ion Medical Machine (HIMM) in Wuwei. Monte Carlo simulations using PHITS were performed for a conservative case under the conditions of maximum beam energy and intensity provided by the HIMM facility. The geometry and configuration of Treatment Room 2 of the HIMM facility in Wuwei were adopted. We evaluated the activation of air, the phantom, and the components of the beamline, such as the primary collimator (PC), ridge filter (RF), and multileaf collimator (MLC). For air activation, we calculated the medical staff immersion external exposure and inhalation internal exposure caused by the corresponding radionuclides. For phantom activation, we estimated the additional dose to the patient's family members owing to secondary photons after treatment. In addition, the exemption or non-exemption of the component material activation was assessed. The results showed that external radiation caused by air activation was the main source of the annual effective dose at approximately 0.5 mSv/y. The induced radioactivity exposure to family members of a patient after CIRT was approximately 40 μSv, sufficiently lower than the public dose limit of 1 mSv/a. The induced radioactivity of the PC, RF, and MLC was all above the exempt levels after the devices were retired, whereas the induced radioactivity of the RS and compensator could reach the exempt levels after one patient session. Our study indicated that medical staff engaged in CIRT should stay away from the high-dose-rate area of induced radioactivity along the beam direction, shorten the residence time in the treatment room as much as possible, and store the activated components in isolation after the equipment is out of use. Thus, this study provides guidance for accurately assessing the level of induced radioactivity in the treatment room for CIRT.

Keywords Induced radioactivity · Monte Carlo · CIRT · PHITS

1 Introduction

Compared to photons, heavy charged particles such as carbon ions simultaneously provide inverted depth-dose distributions and high relative biological effectiveness (RBE)

This work was supported by the National Natural Science Foundation of China (Nos. 12005271 and 12005273), the National Key Research and Development Program of China (No. 2022YFC2401500), and the Western Talent Program of the Chinese Academy of Science (No. 29Y86205).

✉ Qiang Li
liqiang@impcas.ac.cn

✉ Zhong-Ying Dai
daizhongying@impcas.ac.cn

[1] Institute of Modern Physics, Chinese Academy of Sciences, Lanzhou 730000, China

[2] University of Chinese Academy of Sciences, Beijing 100049, China

[3] Key Laboratory of Heavy Ion Radiation Biology and Medicine of Chinese Academy of Science, Lanzhou 730000, China

[4] Key Laboratory of Basic Research on Heavy Ion Radiation Application in Medicine, Lanzhou 730000, China

[5] Lanzhou University, Lanzhou 730000, China

for cancer radiotherapy [1]. These properties make heavy ions more destructive to the target volume and less injurious to surrounding healthy tissues. Statistics from the Particle Therapy Co-Operative Group (PTCOG) show that by the end of 2020, more than 290,000 patients have been treated worldwide with particle therapy, 40,000 of whom were treated with carbon ions, accounting for 13.8%, indicating that carbon-ion radiotherapy (CIRT) plays an increasingly important role in particle therapy. China has also been vigorously developing CIRT, and carbon-ion particle therapy systems have begun construction in places such as Fujian and Zhejiang [2]. As a result, the issue of radiation protection in CIRT has received more attention because high-energy therapeutic carbon-ion beams are necessary for deep-seated tumor treatment to increase radioactivity. The induced radioactivity caused by the bombardment of therapeutic beams on the materials of the treatment room during CIRT gives medical staff and patients unwanted radiation doses [3]. Because induced radioactivity is often the main source of radiation dose for radiotherapy-related staff, it plays a significant role in radiation protection in the treatment room.

The physical basis of induced radioactivity is a nuclear reaction, and the induced radioactivity can only be produced when the conditions of the nuclear reaction are satisfied. For incident neutrons, there are nuclear reactions regardless of energy because neutrons are unstable outside the nucleus and are always captured by other nuclei to stimulate nuclear reactions. However, for other particles, either their energy must reach the reaction threshold for neutron generation or their energy must be sufficiently large to cause nuclear fragmentation [4]. The energy range for CIRT is generally 80–430 MeV/u. Under such high beam energies, the above conditions for the occurrence of a nuclear reaction can be fully satisfied. High-energy therapeutic carbon-ion beams produce secondary particles owing to inelastic nuclear interactions in the devices of beam delivery systems, patients, etc. [5, 6]. Most, but not all, of the radionuclides produced are short lived. Isotopes that are neutron deficient are likely to decay by positron emission or electron capture (EC), and isotopes with excess neutrons are likely to decay by β^- emission. Because many of these decays result in isotopes in an excited state, gamma rays are subsequently emitted, thereby causing exposure to those present in the treatment room [7]. The Shanghai Proton and Heavy-Ion Center (SPHIC) assessed the occupational exposure of medical staff in clinical practice due to the radioactivity induced in patients' tumors to be approximately 0.508 mSv [8]. Although the dose level caused by the induced radioactivity is low, this unwanted radiation should be minimized owing to stochastic effects. Therefore, it is necessary to study the generation mechanism and spatial and temporal distribution characteristics of the induced radioactivity in the treatment room comprehensively, which is important to understand the radiation hazards correctly, formulate protection measures appropriately, and ensure safety during radiotherapy and quality assurance.

This study conducted a more systematic investigation on the induced radioactivity in the treatment room for CIRT using the Monte Carlo (MC) method after consulting literature [9]. The Institute of Modern Physics (IMP), Chinese Academy of Sciences, developed China's first medical carbon-ion therapy system, called the Heavy-Ion Medical Machine (HIMM), in Wuwei. At present, the HIMM facility has entered the stage of clinical application at Wuwei Heavy-Ion Hospital. In this study, the geometry and configuration for the MC simulation were established based on the parameters of the horizontal beamline with a passive beam delivery system in Treatment Room 2 of the HIMM facility in Wuwei. The specific beam model establishment, parameter settings, and calculation formulas are explained in detail in the second section of this paper. The third section highlights the simulation and calculation results, from which some important conclusions of this study were drawn. This study evaluated the induced radioactivity and secondary exposure of medical staff, the public, and patients' families in treatment rooms and provided some radiation protection recommendations. In addition, the degree of activation of different materials under heavy-ion irradiation was assessed to provide a reference for the disposal of out-of-service devices. The aim of this study was to provide guidance for assessing the induced radioactivity level in a radiotherapy treatment room for CIRT.

2 Materials and methods

2.1 Overview of PHITS

PHITS is an MC program package used for studying the transport of particles and heavy ions. The energies of the heavy ions studied ranged from 10 to 100 GeV/u, and the particle types included all the ions (nuclei, nucleons, photons, electrons, muons, etc.) [10, 11]. Due to the feasibility of PHITS for ions transport, this MC program package is commonly used in heavy-ion therapy, space radiation, and radiation protection of heavy-ion accelerators. Applying the CIRT simulation, PHITS has successfully reproduced the dose distribution, including out-of-field doses, and the production of secondary neutrons has been verified in comparison with experiments [12–15].

The calculation of activation in PHITS must be combined with the DCHAIN-PHITS program (referred to as DCHAIN for brevity). DCHAIN is a decay chain analysis code for simulating the production, buildup, burnup, and decay of nuclides as a function of time in any radiation environment. PHITS provides DCHAIN with a neutron flux spectrum

and nuclides generated by high-energy nuclear reactions. DCHAIN performs decay chain analysis, ultimately outputting time-dependent nuclide inventories, decay heat, photon spectra, and effective dose rates [16]. Toyohara et al. calculated the radioactivity using the PHITS code and related code DCHAIN to analyze the experimental results. The results showed that the ratio of the simulated radioactivity to the measured radioactivity was within the range 0.9–1.5 [17]. Therefore, it is reasonable to use PHITS and DCHAIN to calculate the induced radioactivity in this study.

The [T-DCHAIN] tally is defined in PHITS to generate the input file of DCHAIN. In this simulation, we set the intermittent irradiation mode according to the actual situation (8 s for one pulse: 2 s beam-on, 6 s beam-off), and the total irradiation time was 20 min. The DCHAIN calculation relies on two primary types of nuclear dates: neutron reaction cross sections and decay dates. The data libraries we chose were hybrid data libraries. The neutron reaction cross section library was JENDL/AD-2017 + FENDL/A-3.0 + JENDL-4.0 + ENDF/B-VIII0.0 + JEFF-3.3, and the decay data library was JENDL/DDF-2015 + ENDF/BVIII0.0 + ENSDF. In this study, we adopted PHITS version 3.28 [18].

2.2 MC simulation

There are four treatment rooms at the HIMM facility in the Wuwei Heavy-Ion Hospital. The first treatment room contains a horizontal beamline with a spot scanning system, and the second treatment room provides both horizontal beam and vertical passive beam delivery systems. The third treatment room provides a vertical beamline, and the fourth room contains a 45° oblique beamline, both of which are equipped with passive beam delivery systems [19] (Fig. 1a). In this study, a simplified horizontal beamline from the second treatment room was established as the model basis. The dimensions of the treatment room model were 1130 cm × 1698 cm × 600 cm, and the filling material of the wall was standard concrete with a density of 2.3 g/cm^3. The model was determined with reference to computer-aided design (CAD) drawings of the treatment room [20]. The simulation of the beamline included a pre-collimator (PC), ridge filter (RF), and multileaf collimator (MLC). The phantom was a 20 cm × 20 cm × 30 cm water tank irradiated by a 15 cm × 15 cm irradiation field with 2 cm SOBP, which was located at the isocenter of the treatment room. Several idiosyncratic components (such as the compensator and range shifter) were omitted from the simulations for general calculation. However, all of these idiosyncratic components were considered for the evaluation of material activation. In conclusion, we adapted two simplified beamlines to achieve the different aims of this study (Fig. 1b, c). The transport of 1×10^8 carbon ions from the surface of the phase space file was simulated to achieve statistical uncertainties of within 5% for most statistics, although this came at the cost of increasing the CPU computing time [21]. (At some measurement points, fewer particles pass through, and even a large number of the simulations cannot reduce the measurement error at these points.) For conservative consideration, the maximum beam current parameters of the HIMM facility in Wuwei were selected for this simulation. A beam energy of 400 MeV/u was chosen, and the current intensity was 4×10^8 pps. The main beam parameters of the HIMM are listed in Table 1, where the maximum depth corresponds to the range of the carbon-ion beam in water at a maximum energy of 400 MeV/u accelerated by the HIMM facility.

To achieve the research objectives, some measurement points must be set in the simulation. The measurement points were set up every 50 cm from the isocenter in three different directions for a total of nine measuring points (the distribution of the measurement points is shown in Fig. 1d). The three directions were the beam direction, the direction deviating from the beam by 45° to the right, and the vertical beam direction to the right. In other words, only the radiation field on one side was considered. The temporal curves of the dose rates of induced radioactivity at these nine measurement points were output to describe the spatial distribution and temporal change in the induced radioactivity in the treatment room. In addition, 30 cm from the surface of the water phantom was also a point of interest for evaluating the dose caused by the activated phantom to the patient's family members.

2.3 Data analysis method

2.3.1 Calculation of the dose caused by activated air to medical staff

The dose caused by activated air to medical staff includes the internal radiation dose (can be divided into ingestion and inhalation) and external radiation dose (can be divided into air immersion external irradiation, surface deposition external irradiation, and water immersion external irradiation). In this study, combined with the actual situation in the treatment room, we considered only inhalation internal irradiation and air immersion external irradiation. The activity-dose conversion factor of the air immersion external exposure and inhalation dose conversion factor used in the calculation process can be found in the ICRP reports [22, 23] or GB18871-2002 [24].

The dose due to air activation in the treatment room is often characterized by estimating the annual effective dose, which is the main source of professional radiation doses to medical staff. The external immersion irradiation dose is considerably higher than the internal radiation dose. Therefore, the annual effective dose to the medical staff from external exposure to air immersion was the focus of this study to assess the level

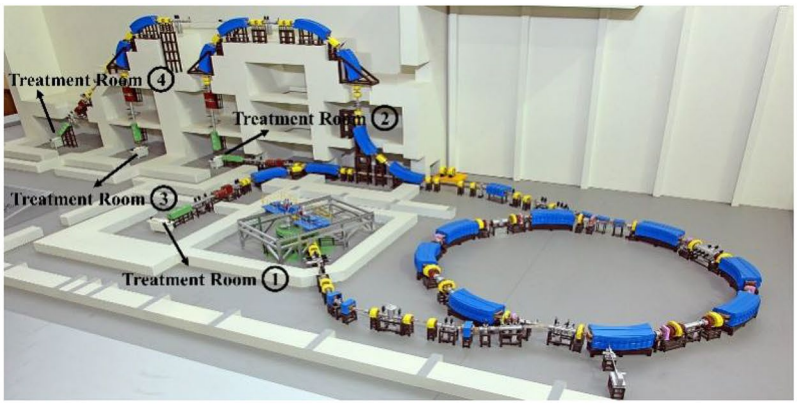

(a)

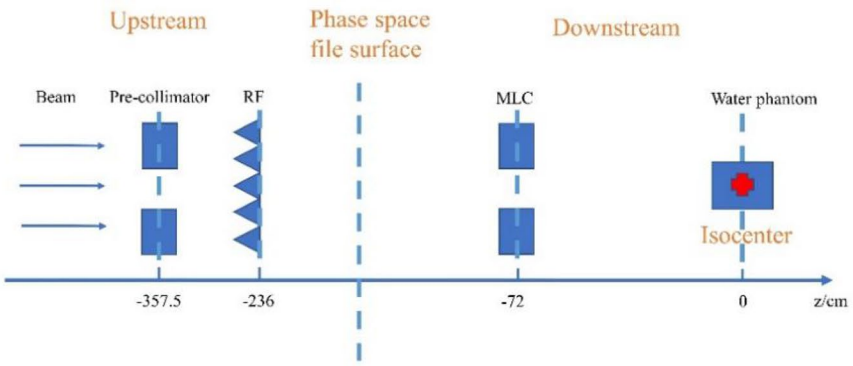

(b)

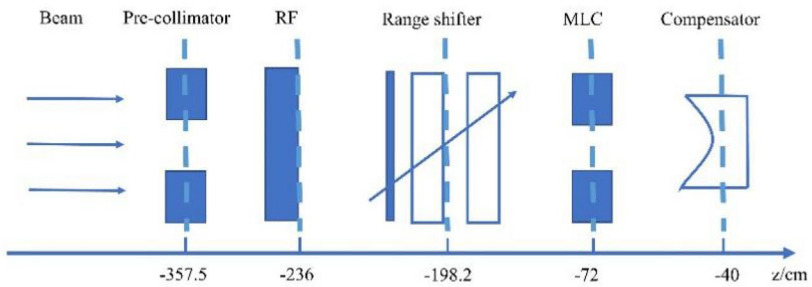

(c)

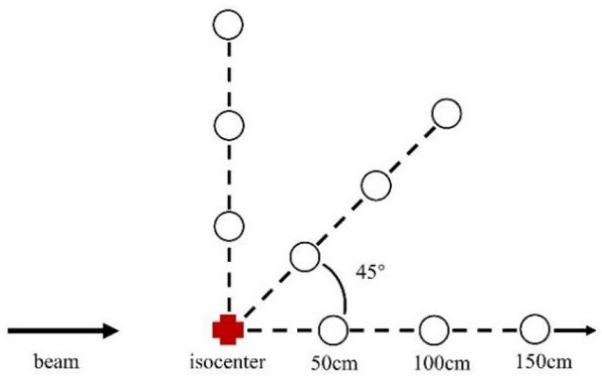

(d)

Fig. 1 (Color online) MC simulation. **a** Heavy-Ion Medical Machine (HIMM); **b** Simplified horizontal beamline for general calculation; **c** Simplified horizontal beamline for material activation assessment; and **d** Distribution of measurement points

Table 1 Main beam parameters of the HIMM

Ion type	^{12}C
Maximum energy (MeV/u)	400
Beam intensity	2×10^{6}–4×10^{8}
Maximum depth (mm)	27.0
Dose uniformity (50×50 mm^2)	95%
Dose rate (Gy/s)	0.001–1.0
Beam size (mm)	$\leq$12.0
Depth step (mm)	2.0

of induced radioactivity in the treatment room. The radionuclides in the air of the treatment room are mainly derived from thermal neutron capture. First, the concentration of each radionuclide induced by radiation in air was calculated using the PHITS simulation program. Then, by superimposing the exposure dose from each induced radionuclide, the external immersion irradiation dose to the medical staff caused by the activated air was obtained. In this study, the concentration of each radionuclide in air was compared with the corresponding derived air concentration (DAC) limit.

The calculation formula of the annual effective dose of external exposure caused by activated air to the medical staff is as follows:

$$E_{\mathrm{imm}} = t_{\mathrm{work}} \times C \times f_{\mathrm{imm}}, \tag{1}$$

where E_{imm} is the annual effective dose of external exposure caused by activated air (in units of Sv/a), t_{work} is the annual working time of the medical staff (in units of h), C is the activity of radionuclides (in units of Bq/m^3), and f_{imm} is the air immersion external radiation dose conversion factor (in units of (Sv/s)/(Bq/m^3)). Because there was an exhaust system in the treatment room, the radionuclide decay constant was corrected for in this dynamic situation to:

$$\lambda = \lambda_i + F/V, \tag{2}$$

where λ_i is the decay constant of the corresponding radionuclide i (in units of s^{-1}), F is the exhaust air velocity of the site, the exhaust rate of Treatment Room 2 is 1.25 m^3/s (4500 m^3/h), and V is the site volume. At the same time, the waiting time t_0 (in units of min) for the medical staff to enter the room after beam stopping and the stay time t (in units of min) for each entry into the treatment room are introduced. Equation (1) then becomes:

$$E_{\mathrm{imm}} = C \times \frac{1}{\lambda} e^{-60\lambda t_0} \times \left(1 - e^{-60\lambda t}\right) \times n \times f_{\mathrm{imm}}, \tag{3}$$

where n is the number of times the medical staff enter the treatment room per year, which is 5000 per year (20 per day).

The annual effective dose due to the inhalation of air containing radionuclides D_{inh}(Sv/a) can be estimated using the following formula:

$$D_{\mathrm{inh}} = XB_{\mathrm{r}}C_{\mathrm{inh}}, \tag{4}$$

where X is the inhaled air nuclide concentration (in units of Bq/m^3), C_{inh} is the inhaled dose conversion factor (in units of Sv/Bq), and B_{r} is the annual volume of air breathed (in units of m^3/a), calculated at a rate of 20 L/min. This part of the calculation does not consider the decay of radionuclides in the air when staying in the treatment room and uses the activity concentration of the radionuclides when entering the treatment room to obtain a conservative value of the annual effective dose of inhalation internal irradiation.

2.3.2 Calculation of the dose caused by the activated phantom to family members

To evaluate the dose to the patient's family members, the following formula was applied:

$$H = \int_{t_1}^{t_2} 2\dot{H}\mathrm{d}t \backsim \mathbf{1}' \tag{5}$$

where $\dot{H}$ is the gamma-ray dose rate 30 cm from the surface of the water phantom. In addition, the following scenario was assumed: The patient leaves the treatment room 2 min after the end of irradiation, and a member of his/her family attends him/her for 2 h. Therefore, t_1 is 2 min, and t_2 is 2 h. Patients receiving CIRT are typically irradiated in fractions of 20–30 irradiations, at most. The total exposure is obtained on the safe side by multiplying the integrated value of Eq. (5) by 30 [25].

2.3.3 Exemption

If the activity of a radionuclide is less than its exemption value, it is called an exempt nuclide. If a substance contains more than one radionuclide and the sum of the ratio of the activity of each radionuclide to their respective exemption value is less than one, the substance is also exempt. In other words, we must determine whether the following equation holds:

$$\sum_i \frac{C_i}{C_{i\mathrm{exp}}} < 1. \tag{6}$$

The exempt activity of radionuclides ($C_{i\mathrm{exp}}$) can be found in GB1887-2002. In this study, the degree of activation of the material was roughly determined by calculating and analyzing whether the sum of the ratios satisfied the above equation [26].

3 Results and discussion

In the present study, three aspects of the induced radioactivity in the treatment room were evaluated: the activation of air in the treatment room, the phantom, and the components of the beamline. After treatment, the medical staff must enter the treatment room for further surgery. The activated air in the treatment room causes external immersion irradiation to the staff, while the inhaled activated air causes internal irradiation. We estimated the occupational exposures of these two components for different waiting and lingering times and compared them with the national standard. The patient's family might also be exposed to additional radiation due to patient activation after treatment; therefore, we estimated this risk and compared it with the standard. The degree of activation of the equipment guides its decommissioning; therefore, we also performed an exemption evaluation of the beamline components. This study can provide a reference for the treatment and disposal of beamline equipment after treatment room dismantling, and we also provide our own recommendations.

3.1 Estimation of air activation

3.1.1 Overview of the air activation situation

As mentioned in the second section, we set up nine measurement points to reflect the spatial distribution of the dose rate of the induced radiation in the treatment room and its variation over time. Figure 2 illustrates the dose rates at each point at different times: 0, 1, 2, 3, 4, 5, 6, 7, 8, 9, 10, 15, 20, 25, and 30 min after irradiation. As shown in these charts, the dose rates of each measurement point in the beam direction were significantly higher than the corresponding measurement points in the 45° direction and those in the direction perpendicular to the beam direction. The dose rates of the latter two orientations were similar, except at the point of 50 cm, where the dose rate in the 45° direction was significantly higher than that at other points. The dose rate decreased with increasing distance. However, in the 0° direction, the decreasing trend of the dose rates with increasing distance was not obvious, unlike in the other two directions. These facts coincide with the particle flux distribution in the treatment room.

The trend of the change in dose rate over time was consistent with the trend of change with distance, which decreased with time. Furthermore, the dose rates of each measurement point in the 45° and 90° directions decreased sharply within 1 min after beam-off and then, slowed down. A large number of radionuclides are generated owing to nuclear reactions during irradiation, and most of these nuclides are short lived with a half-life of less than 1 min. Owing to the low scattering of heavy ions, there were few particles in the non-beam direction, and the probability of a nuclear reaction was also low. The effect of short-lived radionuclides in the non-beam direction on the induced radiation dose rate was considerably greater than that in the beam direction. In the 0° beam

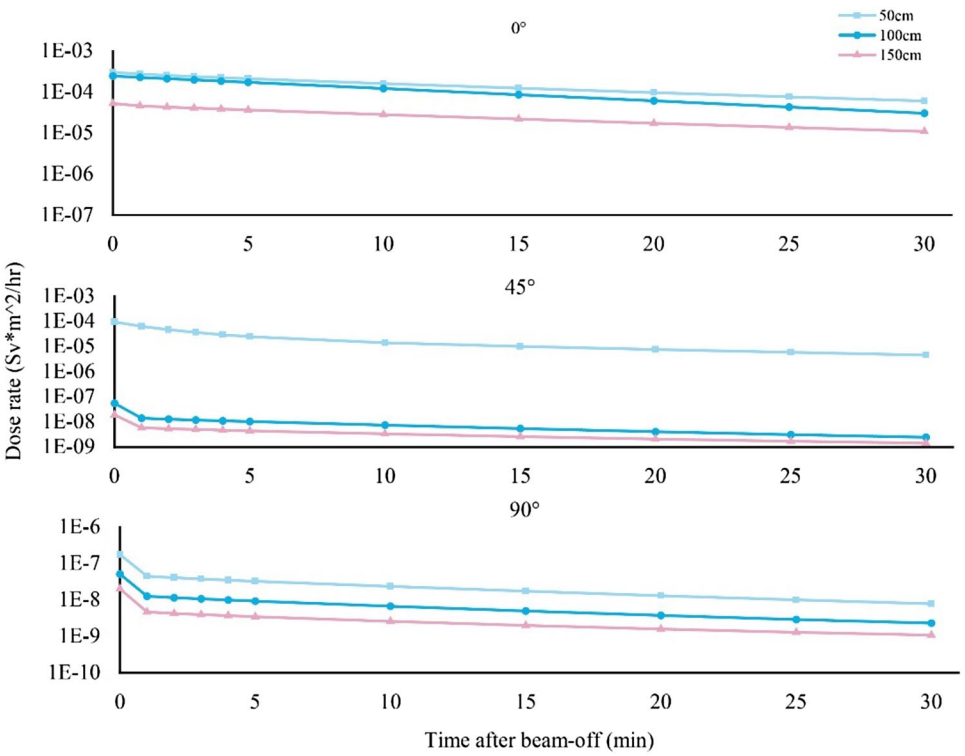

Fig. 2 (Color online) Variation in the dose rate with time at the nine measurement points in the treatment room

direction, the time course of the dose rate was not as fast as in the other two directions, as shown in Fig. 2.

Overall, the distribution of the induced radioactivity in the treatment room was not uniform, and the higher dose-rate area of the residual radiation field was mainly concentrated along the beam direction. Based on the trends from the simulation data and considering the principle of optimization of radiological protection, it is recommended that medical staff should try to avoid the high dose-rate area near the isocenter along the beam direction when entering the treatment room.

3.1.2 Annual effective dose to medical staff caused by air activation

The activity concentrations of each radionuclide at the end of irradiation were first compared with the DAC limits. DAC is the limit of the concentration of radionuclides in the air based on the annual intake limit (ALI), which indicates that the exposure of occupational personnel working in this environment should comply with regulations on the dose equivalent limit [26, 27]. Compared with the corresponding DAC limits, the activity concentration of each nuclide was lower than the corresponding DAC values in this simulation (Table 2). This simulation did not consider the indoor ventilation problem during treatment and obtained a relatively conservative nuclide activity concentration. In this case, the phenomenon in which the radionuclide concentration is lower than the corresponding DAC value can prove that the radionuclide distribution in the air of the treatment room after CIRT complies with radiation protection regulations.

In the second section, we present a formula for calculating the external immersion irradiation dose and internal inhalation irradiation dose in the treatment room. According to the formula given above, the annual effective doses of external immersion irradiation and internal inhalation irradiation caused by air activation in the treatment room to the medical staff were calculated, and the results are listed in Table 3. The number of times the medical staff enter the treatment room was assumed to be 5000 per year (or 20 per day). The value of the internal inhalation irradiation dose was three orders of magnitude smaller than the external radiation dose, which is still under the condition of a conservative calculation. Therefore, we believe that the dose generated by activated air principally originates from external irradiation. If medical staff enter the treatment room immediately after finishing the treatment, the annual effective dose of external radiation is 0.379–0.4107 mSv caused by air activation; 5 and 10 min after beam-off, the annual effective dose is reduced to 0.0948–0.1051 mSv and 0.0092–0.0104 mSv, respectively. According to Chinese Standard GB18871-2002, the occupational annual dose limit is 20 mSv [24]. None of these data exceeded the personal dose limits for professionals stipulated in the basic standards.

Overall, the external exposure dose is an important consideration when calculating the annual effective dose owing to air activation. From the estimation results, it was concluded that suspending entry into the treatment room after the stop could result in a reduction in the annual effective dose of external immersion irradiation caused by activated

Table 3 Annual effective dose to medical staff due to radioactivity of main nuclides activated in indoor air

Waiting time, t_0(min)	Residence time, t (min)	Annual effective dose	
		External radiation (mSv/a)	Internal radiation (mSv/a)
0	10	0.3790	1.695×10^{-4}
0	20	0.4077	3.390×10^{-4}
0	30	0.4107	5.085×10^{-4}
5	10	0.0948	6.240×10^{-5}
5	20	0.1041	1.248×10^{-4}
5	30	0.1051	1.872×10^{-4}
15	10	0.0092	8.500×10^{-6}
15	20	0.0102	1.690×10^{-5}
15	30	0.0104	2.540×10^{-5}

Table 2 Radioactivity of main nuclides and their corresponding DAC values

Nuclide	λ (s^{-1})	Activity concentration (Bq/m^3)	f_{imm} (Sv/s)/(Bq/m^3)	C_{inh} (Sv/Bq)	DAC (Bq/m^3)
H-3	2.7778×10^{3}	1.0269×10^{-2}	–	1.8000×10^{-11}	8.00×10^{5}
Be-7	2.7779×10^{3}	3.7382×10^{-2}	2.7400×10^{-15}	5.2000×10^{-11}	3.00×10^{5}
C-11	3.3445×10^{3}	2 Activity concentration.9122×10^{2}	7.9100×10^{-14}	2.2000×10^{-12}	1.00×10^{7}
C-14	2.7778×10^{3}	1.4547×10^{-4}	2.4300×10^{-16}	6.5000×10^{-12}	–
N-13	3.9371×10^{3}	2.8093×10^{3}	8.6800×10^{-14}	–	7.00×10^{4}
O-15	8.4500×10^{3}	6.3413×10^{3}	1.0400×10^{-13}	–	7.00×10^{4}
S-35	2.7779×10^{3}	4.2487×10^{-11}	2.9200×10^{-16}	1.1000×10^{-9}	–
Cl-38	3.0880×10^{3}	2.0354×10^{-3}	1.9400×10^{-13}	7.0300×10^{-11}	6.00×10^{5}
Cl-39	2.9856×10^{3}	1.5180×10^{-1}	1.3600×10^{-13}	7.6000×10^{-11}	8.00×10^{5}
Ar-41	2.8832×10^{3}	7.1297	1.0100×10^{-13}	–	–

air to medical staff. Therefore, a delay of an appropriate period after radiotherapy is recommended by the optimization principle of radiation protection before radiotherapy staff enter the treatment room.

3.2 Estimation of exposure to the patient's family members from the activated phantom

Patient activation is not traditionally of concern with older photon-based treatments, but is becoming increasingly relevant as high-energy ion treatments have gained prominence because their spallation products and reactions from secondary neutrons result in notable activation [16]. In this study, the patient's own activation and possible additional dose to relatives after receiving CIRT were estimated based on the activation of the phantom used in the simulation.

A large number of radionuclides were generated within the phantom during the simulation. Most of them were short-lived nuclides, which existed only during beam irradiation before decaying. After therapeutic irradiation, the main nuclides in the phantom were O-15, O-14, C-11, N-13, and C-10, which originated mainly from the spallation reaction of O-16 caused by high-energy neutrons. After rapid decay of O-15, O-14, and C-10, C-11 and N-13 became the dominant radionuclides approximately 10 min after irradiation. In addition, there was also an increase in the proportion of other nuclides after 20 min, as shown in Fig. 3. These were mainly nuclides with relatively long half-lives, such as H-3 and Be-7.

Table 4 Main radionuclides in the phantom after irradiation

Nuclide	Half-life (s)	Decay mode
O-15	1.22×10^{2}	EC, β^{+}
O-14	7.06×10^{1}	EC, β^{+}
C-11	1.22×10^{3}	EC, β^{+}
N-13	5.98×10^{2}	EC, β^{+}
C-10	1.93×10^{1}	EC, β^{+}
H-3	3.89×10^{8}	β^{-}
Be-7	4.60×10^{6}	EC

As shown in Table 4, EC and β decay were the dominant decay modes, whereas positron annihilation from β^{+} decay emitted photons. Because beta rays are less penetrating, only the secondary photon dose due to material activation was considered while considering the water phantom activation. The calculated photon spectra from the irradiation phantom were used as the input source term for a secondary-stage calculation to assess the dose from the activated materials. The time-dependent changes in the secondary photon dose rate due to phantom material activation in the treatment room are shown in Fig. 4. When the phantom was radioactivated by carbon ions, it emitted radiation rays into its surroundings from the center of the phantom. The secondary photon dose decreased with increasing distance from the phantom. The maze structure of the treatment room has a good shielding effect, which significantly reduces the dose rates at the entrance and corridor of the maze. However, there is no similar shielding structure between family members

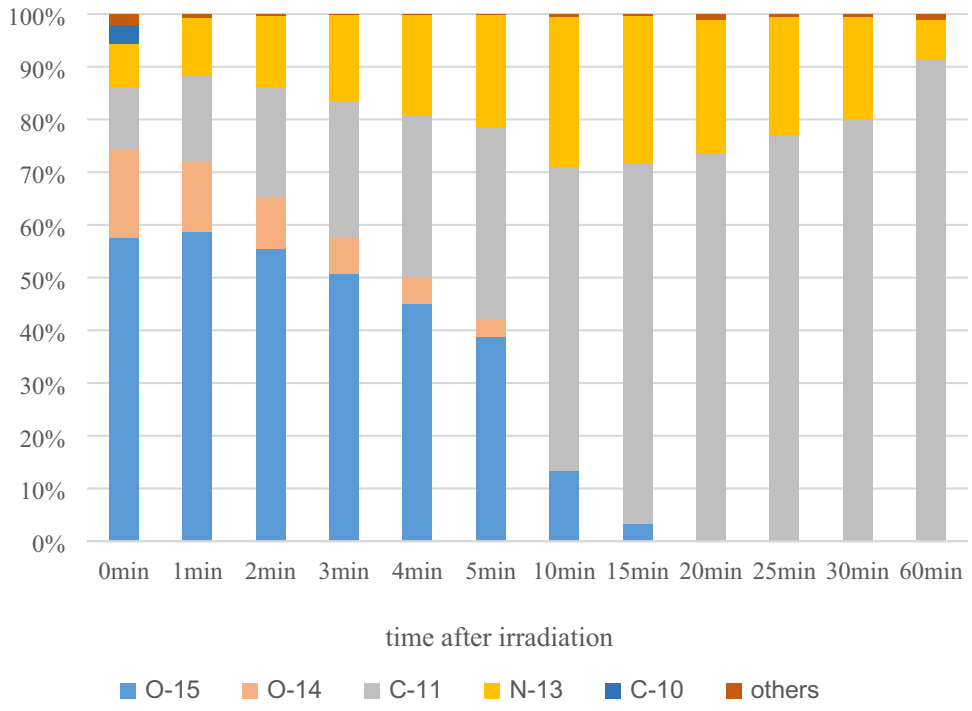

Fig. 3 (Color online) Simulation results of induced radionuclides and the ratio of their activities from 0 to 60 min after irradiation

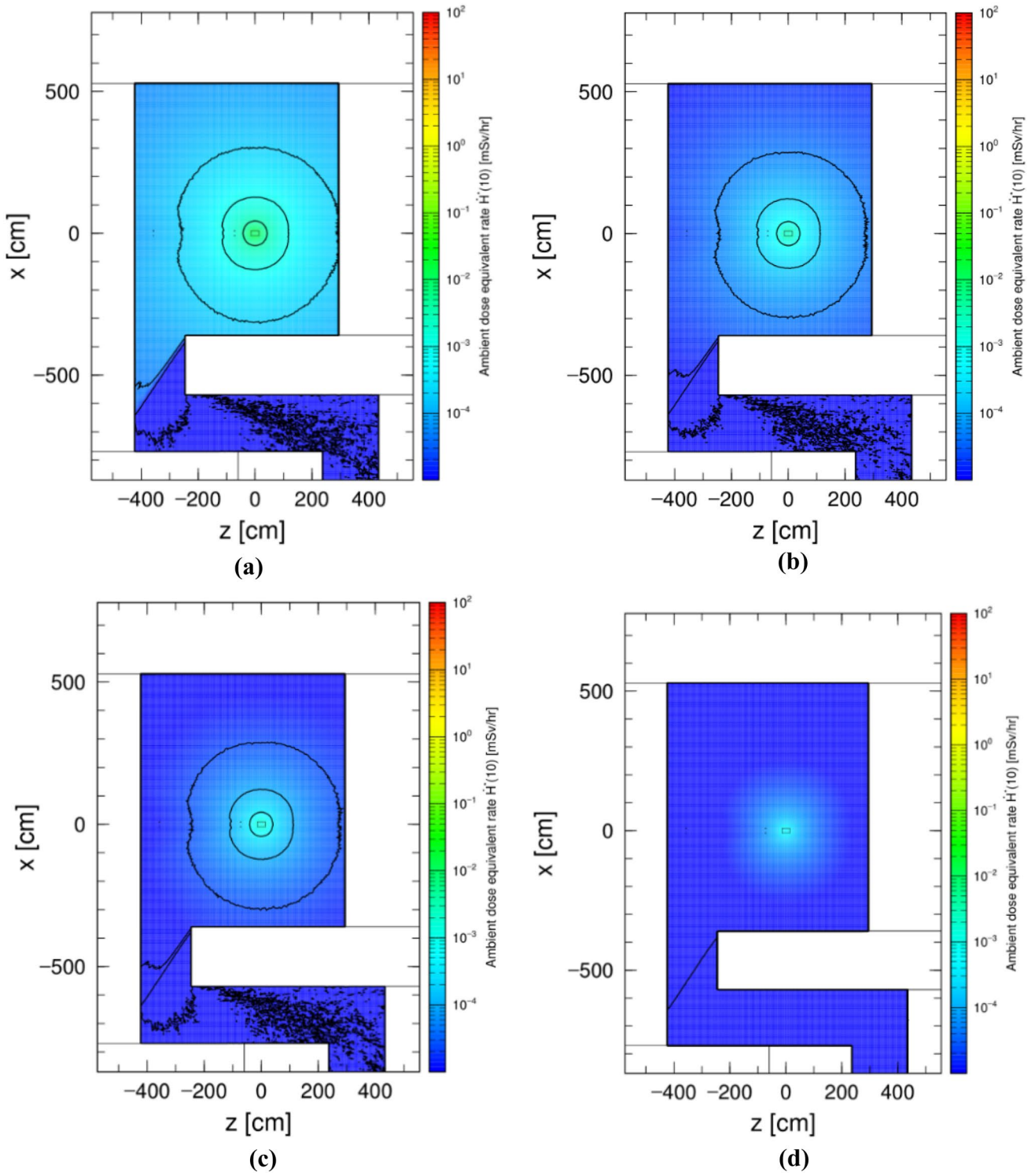

Fig. 4 (Color online) Variation in the secondary photon dose-rate distribution with time in the treatment room. **a** 0 min after beam stop; **b** 5 min after beam stop; **c** 10 min after beam stop; and **d** 30 min after beam stop

and patients after CIRT, and the photon dose-rate levels around the patient are at a relatively high level immediately after one exposure; therefore, it is necessary to estimate the additional dose to family members due to activation of patients who receive CIRT (Fig. 5).

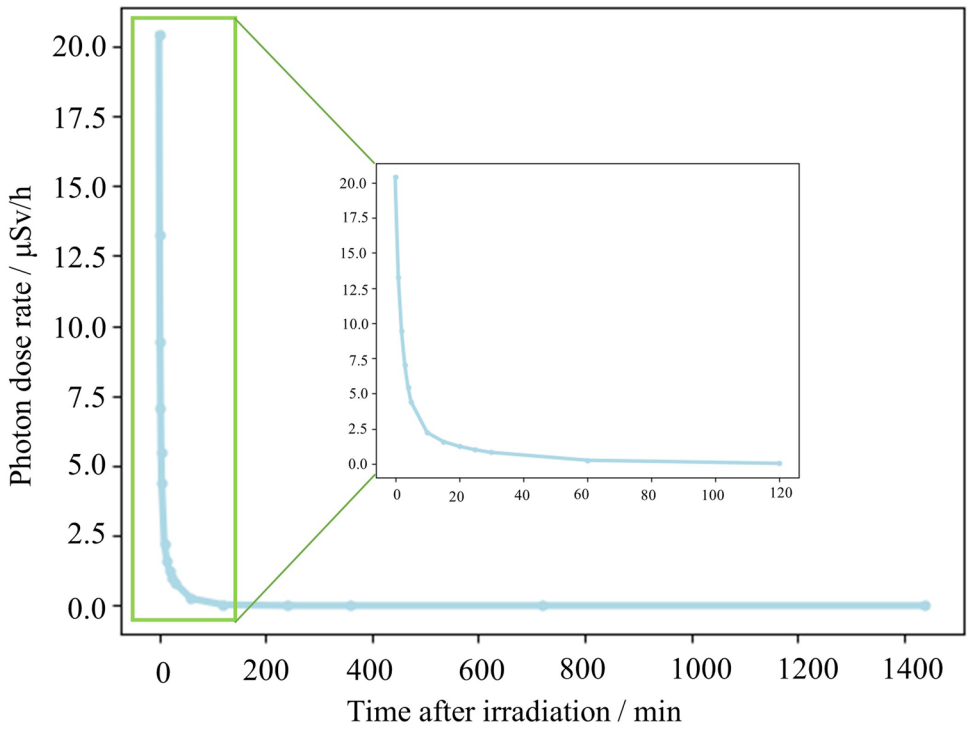

Fig. 5 Variation in the secondary photon dose rate with time at the measurement point

The exposure to family members was calculated as 40 μSv for the HIMM using Eq. (5). Compared with 23.5 μSv for the HIMAC of the National Institute of Radiological Sciences (NIRS) and 20.8 μSv for the Hyogo Ion Beam Medical Center (HIBMC) [25], our calculation was almost twice as high. This is mostly because we adopted the maximum beam parameters of the HIMM in the simulation and obtained relatively conservative data. Most radioactive nuclides produced in phantoms have very short half-lives. Therefore, even if family members attend to the patient for a prolonged time, the exposure hardly increases. In ICRP publication 103, this type of exposure is classified as medical exposure; therefore, the public dose limitation is not suitable for use in this case [28]. However, based on the results of our calculation, the exposure to the family members of a patient is far less than the public dose limit of 1 mSv/a; therefore, this extra radiation does not have much impact on the patient's family.

3.3 Material activation analysis

Primary and secondary particles react with the components of the beamline to generate large amounts of radionuclides, which activate the material. Assessing the activation level of the beamline components is important to guide equipment decommissioning. To simplify the simulation, simple geometries were used to replace the complex beamline components, and the specific parameters are listed in Table 5. We divided the components into two categories: fixed and nonfixed components. For the fixed components (the PC, RF, and MLC), we set a continuous exposure of 30 years using the maximum flow intensity. For range shifters and compensators with patient specificity, we only considered the activation after one patient session. Continuous irradiation for 20 min was followed by cooling for 24 h. This was repeated 30 times for one patient session. The activity concentrations of major activated nuclides of each component are given in Tables 6, 7, 8, 9, 10.

Table 5 Material of each equipment in the beamline

Component	Material	Density (g/cm^3)	Open field (cm^2)
PC	Cu	8.960	15×15
RF	Al	2.700	–
RS	PMMA	1.190	–
MLC	Cu 5% W 95%	18.230	15×15
Compensator	Polyethylene	0.942	–

For the fixed components, a large number of radionuclides were generated after irradiation, particularly the MLC. Many of these radionuclides were short lived. However, these are less important for radiation protection. Therefore,

Table 6 Main nuclides of the PC

Nuclide	Activity (Bq)	Exempt	Activity/Exempt	Half-life (s)
Ni-63	4.06×10^{5}	1.00×10^{8}	4.06×10^{-3}	3.19×10^{9}
H-3	4.66×10^{6}	1.00×10^{9}	4.66×10^{-3}	3.89×10^{8}
Co-60	9.61×10^{5}	1.00×10^{5}	9.61	1.66×10^{8}
Fe-55	9.17×10^{5}	1.00×10^{6}	9.17×10^{-1}	8.66×10^{7}
Na-22	5.08×10^{4}	1.00×10^{6}	5.08×10^{-2}	8.21×10^{7}
Mn-54	8.59×10^{5}	1.00×10^{6}	8.59×10^{-1}	2.70×10^{7}
Co-57	1.06×10^{6}	1.00×10^{6}	1.06	2.35×10^{7}
Zn-65	1.29×10^{5}	1.00×10^{6}	1.29×10^{-1}	2.11×10^{7}
Ca-45	8.52×10^{4}	1.00×10^{7}	8.52×10^{-3}	1.41×10^{7}
S-35	1.19×10^{5}	1.00×10^{8}	1.19×10^{-3}	7.56×10^{6}
Sc-46	2.32×10^{5}	1.00×10^{6}	2.32×10^{-1}	7.24×10^{6}
Co-56	2.61×10^{5}	1.00×10^{5}	2.61	6.67×10^{6}
Co-58	1.43×10^{6}	1.00×10^{6}	1.43	6.12×10^{6}
Be-7	1.43×10^{5}	1.00×10^{7}	1.43×10^{-2}	4.60×10^{6}
Fe-59	1.28×10^{5}	1.00×10^{6}	1.28×10^{-1}	3.84×10^{6}
A-r37	1.15×10^{5}	1.00×10^{8}	1.15×10^{-3}	3.03×10^{6}
C-r51	6.08×10^{5}	1.00×10^{7}	6.08×10^{-2}	2.39×10^{6}
P-33	1.36×10^{5}	1.00×10^{8}	1.36×10^{-3}	2.19×10^{6}
V-48	2.65×10^{5}	1.00×10^{5}	2.65	1.38×10^{6}
P-32	1.81×10^{5}	1.00×10^{5}	1.81	1.23×10^{6}
Mn-52	2.12×10^{5}	1.00×10^{5}	2.12	4.83×10^{5}
Ca-47	1.19×10^{4}	1.00×10^{6}	1.19×10^{-2}	3.92×10^{5}
Sc-47	1.84×10^{5}	1.00×10^{6}	1.84×10^{-1}	2.89×10^{5}
Sc-48	6.80×10^{4}	1.00×10^{5}	6.80×10^{-1}	1.57×10^{5}
K-43	6.53×10^{4}	1.00×10^{6}	6.53×10^{-2}	8.03×10^{4}
Co-55	4.80×10^{4}	1.00×10^{6}	4.80×10^{-2}	6.31×10^{4}
Na-24	5.71×10^{4}	1.00×10^{5}	5.71×10^{-1}	5.40×10^{4}
Cu-64	3.60×10^{6}	1.00×10^{6}	3.60	4.57×10^{4}
K-42	1.28×10^{5}	1.00×10^{6}	1.28×10^{-1}	4.45×10^{4}
Fe-52	5.19×10^{3}	1.00×10^{6}	5.19×10^{-3}	2.98×10^{4}
Si-31	6.03×10^{4}	1.00×10^{6}	6.03×10^{-2}	9.44×10^{3}
Mn-56	2.38×10^{5}	1.00×10^{5}	2.38	9.28×10^{3}
Ni-65	1.69×10^{5}	1.00×10^{6}	1.69×10^{-1}	9.06×10^{3}
F-18	6.99×10^{4}	1.00×10^{6}	6.99×10^{-2}	6.59×10^{3}
Ar-41	2.35×10^{4}	1.00×10^{6}	2.35×10^{-2}	6.58×10^{3}
Co-61	5.12×10^{5}	1.00×10^{6}	5.12×10^{-1}	5.94×10^{3}
Mn-51	4.51×10^{4}	1.00×10^{5}	4.51×10^{-1}	2.77×10^{3}
Cl-38	5.74×10^{4}	1.00×10^{5}	5.74×10^{-1}	2.23×10^{3}
Mn-52 m	5.32×10^{3}	1.00×10^{5}	5.32×10^{-2}	1.27×10^{3}
O-15	1.83×10^{4}	1.00×10^{9}	1.83×10^{-5}	1.22×10^{2}

Table 7 Main nuclides of the MLC

Nuclide	Activity (Bq)	Exempt	Activity/Exempt	Half-life (s)
Ni-63	2.64×10^{5}	1.00×10^{8}	2.64×10^{-3}	3.19×10^{9}
H-3	1.82×10^{6}	1.00×10^{9}	1.82×10^{-3}	3.89×10^{8}
Co-60	5.81×10^{5}	1.00×10^{5}	5.81	1.66×10^{8}
Fe-55	4.91×10^{5}	1.00×10^{6}	4.91×10^{-1}	8.66×10^{7}
Na-22	4.68×10^{3}	1.00×10^{6}	4.68×10^{-3}	8.21×10^{7}
Mn-54	4.48×10^{5}	1.00×10^{6}	4.48×10^{-1}	2.70×10^{7}
Co-57	6.03×10^{5}	1.00×10^{6}	6.03×10^{-1}	2.35×10^{7}
Zn-65	7.36×10^{4}	1.00×10^{6}	7.36×10^{-2}	2.11×10^{7}
Ca-45	2.91×10^{4}	1.00×10^{7}	2.91×10^{-3}	1.41×10^{7}
Ce-139	1.96×10^{3}	1.00×10^{6}	1.96×10^{-3}	1.19×10^{7}
W-181	3.08×10^{5}	1.00×10^{7}	3.08×10^{-2}	1.05×10^{7}
Ta-182	6.47×10^{4}	1.00×10^{4}	6.47	9.91×10^{6}
S-35	2.63×10^{4}	1.00×10^{8}	2.63×10^{-4}	7.56×10^{6}
Sc-46	8.59×10^{4}	1.00×10^{6}	8.59×10^{-2}	7.24×10^{6}
Co-56	1.37×10^{5}	1.00×10^{5}	1.37	6.67×10^{6}
W-185	2.49×10^{5}	1.00×10^{7}	2.49×10^{-2}	2.49×10^{5}
Co-58	8.46×10^{5}	1.00×10^{6}	8.46×10^{-1}	6.12×10^{6}
Be-7	1.80×10^{5}	1.00×10^{7}	1.80×10^{-2}	4.60×10^{6}
Fe-59	7.43×10^{4}	1.00×10^{6}	7.43×10^{-2}	3.84×10^{6}
Cr-51	2.80×10^{5}	1.00×10^{7}	2.80×10^{-2}	2.39×10^{6}
V-18	1.03×10^{5}	1.00×10^{5}	1.03	1.38×10^{6}
P-32	3.19×10^{4}	1.00×10^{5}	3.19×10^{-1}	1.23×10^{6}
Mn-52	9.67×10^{4}	1.00×10^{5}	9.67×10^{-1}	4.83×10^{5}
Sc-47	7.05×10^{4}	1.00×10^{6}	7.05×10^{-2}	2.89×10^{5}
Sc-48	2.63×10^{4}	1.00×10^{5}	2.63×10^{-1}	1.57×10^{5}
W-187	2.57×10^{4}	1.00×10^{6}	2.57×10^{-2}	8.64×10^{4}
K-43	2.02×10^{4}	1.00×10^{6}	2.02×10^{-2}	8.03×10^{4}
Co-55	2.27×10^{4}	1.00×10^{6}	2.27×10^{-2}	6.31×10^{4}
Na-24	5.52×10^{3}	1.00×10^{5}	5.52×10^{-2}	5.40×10^{4}
Cu-64	2.22×10^{6}	1.00×10^{6}	2.22	4.57×10^{4}
K-42	3.79×10^{4}	1.00×10^{6}	3.79×10^{-2}	4.45×10^{4}
Si-31	1.04×10^{4}	1.00×10^{6}	1.04×10^{-2}	9.44×10^{3}
Mn-56	1.26×10^{5}	1.00×10^{5}	1.26	9.28×10^{3}
Ni-65	1.03×10^{5}	1.00×10^{6}	1.03×10^{-1}	9.06×10^{3}
F-18	4.81×10^{3}	1.00×10^{6}	4.81×10^{-3}	6.59×10^{3}
Co-61	3.29×10^{5}	1.00×10^{6}	3.29×10^{-1}	5.94×10^{3}
Mn-51	1.95×10^{4}	1.00×10^{5}	1.95×10^{-1}	2.77×10^{3}
Cl-38	1.40×10^{4}	1.00×10^{5}	1.40×10^{-1}	2.23×10^{3}

considering the half-life and activity together, we organized meaningful radionuclides in the table. The RS and compensator produced considerably fewer radionuclides.

For the PC, MLC, and RF, the sum of the ratios of individual nuclides and their corresponding exempt activities was considerably greater than 1. Therefore, the fixed components of the beamline after decommissioning the treatment room must be stored in isolation and disposed of until their radioactivity levels reach exempt levels. The RS and compensator produce weak activity radioactivity and fewer long-lived nuclides because they are materials with a small atomic number. Their activation levels after a patient session were also exempt. However, considering the As Low As Reasonably Achievable (ALARA) principle, we still recommend that they should be placed in isolation at the end of treatment.

Table 8 Main nuclides of the RF

Nuclide	Activity (Bq)	Exempt	Activity/Exempt	Half-life (s)
H-3	3.23×10^{6}	1.00×10^{9}	3.23×10^{-3}	3.89×10^{8}
Be-7	2.99×10^{5}	1.00×10^{7}	2.99×10^{-2}	4.60×10^{6}
C-14	2.60×10^{2}	1.00×10^{7}	2.60×10^{-5}	1.80×10^{11}
O-15	2.01×10^{5}	1.00×10^{9}	2.01×10^{-4}	1.22×10^{2}
F-18	6.52×10^{5}	1.00×10^{6}	6.52×10^{-1}	6.59×10^{3}
Na-22	6.92×10^{5}	1.00×10^{6}	6.92×10^{-1}	8.21×10^{7}
Na-24	7.39×10^{5}	1.00×10^{5}	7.39	5.40×10^{4}
Si-31	3.00×10^{1}	1.00×10^{6}	3.00×10^{-5}	9.44×10^{3}
P-32	4.99×10^{1}	1.00×10^{5}	4.99×10^{-4}	1.23×10^{6}

Table 9 Main nuclides of the RS

Nuclide	Activity (Bq)	Exempt	Activity/Exempt	Half-life (s)
H-3	2.23×10^{2}	1.00×10^{9}	2.23×10^{-7}	3.89×10^{8}
Be-7	4.02×10^{3}	1.00×10^{7}	4.02×10^{-4}	4.60×10^{6}
C-11	1.72×10^{4}	–	–	1.22×10^{3}
C-14	1.65×10^{-2}	1.00×10^{7}	1.65×10^{-9}	1.80×10^{11}
N-13	4.55×10^{1}	–	–	5.98×10^{2}
O-15	2.31×10^{-12}	1.00×10^{9}	2.31×10^{-21}	1.22×10^{2}
F-18	1.34×10^{2}	1.00×10^{6}	1.34×10^{-4}	6.59×10^{3}
Na-22	2.41×10^{-3}	1.00×10^{6}	2.41×10^{-9}	8.21×10^{7}
Si-31	6.92×10^{-17}	1.00×10^{5}	6.92×10^{-22}	9.44×10^{3}

Table 10 Main nuclides of the compensator

Nuclide	Activity (Bq)	Exempt	Activity/Exempt	Half-life (s)
H-3	7.23×10^{1}	1.00×10^{9}	7.23×10^{8}	3.89×10^{8}
Be-7	1.36×10^{3}	1.00×10^{7}	1.36×10^{4}	4.60×10^{6}
Be-10	3.18×10^{-5}	–	–	4.77×10^{13}
C-11	6.23×10^{3}	–	–	1.22×10^{3}
C-14	6.70×10^{5}	1.00×10^{7}	6.70×10^{-12}	1.80×10^{11}
N-13	3.31×10^{-1}	–	–	5.98×10^{2}
O-15	7.97×10^{-16}	1.00×10^{9}	7.97×10^{-25}	1.22×10^{2}
F-18	1.11	1.00×10^{9}	1.11×10^{-9}	6.59×10^{3}
P-33	6.73×10^{-2}	1.00×10^{8}	6.73×10^{-10}	2.19×10^{6}

4 Conclusion

The investigation of non-therapeutic radiation is of vital importance for better radiotherapy efficacy. In a previous study, we analyzed secondary neutron doses under a passive beam delivery system and applied an analytical model to predict the ambient dose equivalent [29]. In this study, we performed a relatively comprehensive analysis of induced radioactivity, which enriched our understanding of non-therapeutic radiation in CIRT. Based on the MC particle transport simulation software PHITS, this study evaluated the activation of air, the phantom, and the components of the beamline in a CIRT treatment room. For air activation, we calculated the medical staff external immersion exposure and internal inhalation exposure caused by the corresponding radionuclides. For phantom activation, we estimated the additional dose to the patient's family caused by secondary photons. For component material activation, we evaluated the exemption or non-exemption. The following conclusions were drawn:

1. After beam-off, the areas with a high dose rate of induced radioactivity in the treatment room were mainly located upstream of the beam direction near the phantom. After entering the treatment room, medical staff should avoid staying in these areas to reduce radiation hazards.
2. The annual evidence dose caused by air activation does not exceed the personal dose limits for professionals stipulated in the basic standards, and the main source is air immersion external radiation. Additionally, after irradiation with radiotherapy, an appropriate time delay before entering the treatment room is recommended.
3. The maze structure of the treatment room can have a good shielding effect, thereby significantly reducing the dose rate of secondary photons caused by the activation of the phantom at the maze entrance and corridor. The dose rate near the phantom was high immediately after beam-off and then, decreased roughly exponentially with time. The possible additional dose to the patient's family, derived from the secondary photons of the present treatment fraction, was estimated to be approximately 40 μSv, which does not have much impact on the patient's family.
4. Beamline components generate large amounts of radionuclides after nuclear reactions with primary and secondary particles. Materials with high atomic numbers produce high levels of induced radioactivity and generate long-lived nuclides. The induced radioactivity of the PC, RF, and MLC is above the exempt levels after the devices are retired, and isolation treatment is required. The RS and compensator can reach the exempt levels after one patient session but should still be placed separately.

The additional radiation caused by the induction radioactivity in Treatment Room 2 of the HIMM is below legal limits. We made recommendations for radiation protection based on the analysis of induction radiation in the treatment room, which are also applicable to other therapy centers with CIRT.

There are several limitations to the simulation setup. A simplified beamline model was used, and devices such as the

patient couch in the treatment room were neglected. Additionally, ventilation in the treatment room during irradiation was not considered. Nevertheless, we believe that our study may provide a framework for other induced radioactivity studies on the CIRT treatment room. Moreover, in future studies, experimental measurements will be performed.

In summary, our study provides references for assessing the induced radioactivity levels in treatment rooms for CIRT and provides several radiation protection recommendations for medical staff and equipment decommissioning. With the popularization of CIRT in China, this study might help different CIRT centers to take action when considering the radiation protection of induced radioactivity. For some new radiotherapy techniques, such as flash, multi-ion combined therapy, and arc therapy, it is also important to re-evaluate the induced radioactivity level under these new radiotherapy techniques. The research methods in this paper also provide guidance for the study of induced radioactivity under these new techniques so that they can be better applied in clinical practice.

Author contributions All authors contributed to the study conception and design. Material preparation, data collection, and analysis were performed by Ying Luo, Sheng-Cong Huang, Hui Zhang, Hai-Jun Mao, Qiang Li, and Zhong-Ying Dai. The first draft of the manuscript was written by Ying Luo, and all authors commented on previous versions of the manuscript. All authors read and approved the final manuscript.

References

1. G. Kraft, RBE and its interpretation. Strahlenther. Onkol. **175**, 44–47 (1999). https://doi.org/10.1007/BF03038887
2. G.Q. Xiao, Q. Li, X.Q. Zhang et al., The development and commercialization of carbon ion cancer therapy facility. J. Innov. China **16**(1), 9–17 (2020). https://doi.org/10.11842/chips.20200310002 (in Chinese)
3. P.J. Gollon, Production of radioactivity by particle accelerators. Nucl. Sci. **23**, 1395–1400 (1976). https://doi.org/10.1109/TNS.1976.4328488
4. F. Lu, C.J. Liu, D.P. Deng, The research status of induced radioactivity in accelerator facilities. Foreign Med. Sci.·Sec. Radiat. Med. Nucl. Med. **29**(6), 297–300 (2005). https://doi.org/10.3760/cma.j.issn.1673-4114.2005.06.017 (in Chinese)
5. K. Gunzert-Marx, H. Iwase, D. Schardt et al., Secondary beam fragments produced by 200 MeV/u ^{12}C ions in water and their dose contributions in carbon ion therapy. New J. Phys. **10**, 1–21 (2008). https://doi.org/10.1088/1367-2630/10/7/075003
6. M. Hultqvist, I. Gudowska, J.-L. Li, Secondary absorbed does from light ion irradiation in anthropomorphic phantoms representing an adult male and a 10 year old child. Phys. Med. Biol. **55**, 6633–6653 (2010). https://doi.org/10.1088/0031-9155/55/22/004
7. B. Thomadsen, R. Nath, F.B. Bateman et al., Potential hazard due to induced radioactivity secondary to radiotherapy: the report of task group 136 of the American association of physicists in medicine. Health Phys. **107**, 442–460 (2014). https://doi.org/10.1097/HP.0000000000000139
8. Z.L. Liu, X.W. Wang, W. Ren, Assessment of occupational exposure doses to physicians in clinical practice at Shanghai proton and heavy ion center. Chin. J. Radiol. Med. Prot. **38**(11), 851–854 (2018). https://doi.org/10.3760/cma.j.issn.0254-5098.2018.11.010 (in Chinese)
9. Z. Wu, J.L. Li, Z. Zeng et al., Calculation method of induced radioactivity in electron linear accelerator. J. Tsinghua Univ. Sci. Tech. **45**(06), 813–816 (2005). https://doi.org/10.16511/j.cnki.qhdxxb.2005.06.025 (in Chinese)
10. G. Mckinney, J. Dragos, J. Hendricks et al., Review of Monte Carlo all-particle transport codes and overview of recent MCNPX features. Proc. Sci. 1–16 (2006). https://doi.org/10.22323/1.025.0088
11. H. Iwase, K. Niita, T. Nakamura, Development of general-purpose particle and heavy ion transport Monte Carlo code. Nucl. Sci. Technol. **39**, 1142–1151 (2002). https://doi.org/10.1080/18811248.2002.9715305
12. E. Haettner, H. Iwase, D. Schardt, Experimental fragmentation studies with ^{12}C therapy beams. Radiat. Prot. Dosim. **122**, 485–487 (2006). https://doi.org/10.1093/rpd/ncl402
13. H. Iwase, K. Gunzert-Marx, E. Haettner et al., Experimental and theoretical study of the neutron dose produced by carbon ion therapy beams. Radiat. Prot. Dosim. **126**, 615–618 (2007). https://doi.org/10.1093/rpd/ncm140
14. S. Yonai, N. Matsufuji, T. Kanai, Monte Carlo study on secondary neutrons in passive carbon-ion radiotherapy: identification of the main source and reduction in the secondary neutron dose. Med. Phys. **36**(10), 4830–4839 (2009). https://doi.org/10.1118/1.3220624
15. S. Yonai, N. Matsufuji, M. Namba, Calculation of out-of-field dose distribution in carbon-ion radiotherapy by Monte Carlo simulation. Med. Phys. **39**, 5028–5039 (2012). https://doi.org/10.1118/1.4736823
16. H.N. Ratliff, N. Matsuda, S. Abe et al., Modernization of the DCHAIN-PHITS activation code with new features and updated data libraries. Nucl. Instrum. Methods Phys. Res. Sect. B **484**, 29–41 (2020). https://doi.org/10.1016/j.nimb.2020.10.005
17. M. Toyohara, S. Minohara, Y. Kusano et al., Induced radionuclides and their activity concentration in gel dosimeters irradiated by carbon ion beam. Gels **8**, 203 (2022). https://doi.org/10.3390/gels8040203
18. T. Sato, Y. Iwamoto, S. Hashimoto et al., Features of particle and heavy ion transport code system (PHITS) version 3.02. Nucl. Sci. Technol. **55**, 684–690 (2018). https://doi.org/10.1080/00223131.2017.1419890
19. H. Zhang, Z.-Y. Dai, X.-G. Liu et al., Research progress on accurate pencil beam model for heavy ion cancer therapy. Nucl. Phys. Rev. **35**, 85–93 (2018). https://doi.org/10.11804/NuclPhysRev.35.01.085
20. X. Wang, J.L. Li, Z. Wu et al., CMGC: a CAD to Monte Carlo geometry conversion code. Nucl. Sci. Tech. **31**, 82 (2020). https://doi.org/10.1007/s41365-020-00793-8
21. Y.H. Zhang, Nonrecursive residual Monte Carlo method for S_N transport discretization error estimation. Nucl. Sci. Tech. **33**, 61 (2022). https://doi.org/10.1007/s41365-022-01042-w
22. ICRP, ICRP publication68: dose coefficients for intakes of radionuclides by workers Ann. ICRP 24(4) (1994)
23. ICRP, ICRP publication74: conversion coefficients for use in radiological protection against external radiation Ann. ICRP 26(3–4) (1996)
24. National Standard, GB18871–2002, Basic standards for protection against ionizing radiation and for the safety of radiation sources, China Standard Press, 2002. (in Chinese)
25. H. Tujii, T. Akagi, K. Akahane et al., Research on radiation protection in the application of new technologies for proton and heavy ion radiotherapy. Jpn. J. Med. Phys. **28**, 172–206 (2009). https://doi.org/10.11323/jjmp2000.28.4_172
26. Y. Yang, Dissertation, Research on key issues of radiation protection of HIAF radioactive secondary beam separation line (HFRS).

University of Chinese Academy of Sciences Institute of Modern Physics, Chinese Academy of Sciences 2020. https://doi.org/10.27560/d.cnki.gkjwc.2020.000016 (in Chinese)
27. J.L. Wang, Radiation protection basic course. Tsinghua University Press, 2012. (in Chinese)
28. ICRP, ICRP the 2007 recommendations of the international commission on radiological protection Ann. ICRP 37(2–4) (2007)
29. S.C. Huang, H. Zhang, K. Bai et al., Monte Carlo study of the neutron ambient dose equivalent at the heavy ion medical machine in Wuwei. Nucl. Sci. Tech. **33**, 119 (2022). https://doi.org/10.1007/s41365-022-01093-z